A trajectory is obtained to a slightly elliptical (parking) orbit with the desired perigee radius without plane change with a 90° launch azimuth. This problem converges easily. Then the ascent burn time is fixed at the value obtained and a variable length parking orbit coast, a fixed parking orbit perigee radius and second burn are added. This problem is targeted to the desired apogee and 180° argument of perigee for first equator crossing second burn. An inclination decrease of about two degrees is then added to these final conditions and the problem is retargeted to the augmented final conditions. Now the transfer orbit coast (variable) and apogee burn (fixed or variable) are added. This trajectory is integrated to the end with the converged initial guesses from the last step. The final conditions achieved will frequently be far from a circular synchronous equatorial orbit. However, specify the final conditions actually achieved as the desired ones, and optimize the problem. The parking orbit coast, second burn, and transfer orbit coast durations will change. Now alter the achieved final conditions toward the desired ones judiciously in steps, retargeting at each step. In this manner, the desired final orbit conditions may be obtained. Now the ascent burn duration may be optimized. Any sizable change in a constraint or final condition is best achieved by proceeding in steps. The problem is quite nonlinear. Attempts to plot initial conditions as functions of the final conditions for extrapolation purposes were made. They were generally unsuccessful.

References

[1] Hoelker, R. F. and Silber, R., "Injection Schemes for Obtaining a Twenty-Four Hour Orbit," *Aerospace Engineering*, Vol. 20, No. 1, Jan. 1961, pp. 28–29, 76–84.

[2] Rider, L., "Characteristic Velocity Requirements for Impulsive Thrust Transfers Between Non Co-Planar Circular Orbits," *ARS Journal*, Vol. 31, No. 3, March 1961, pp. 345–351.

[3] Teren, F. and Spurlock, O. F., "Payload Optimization of Multi-stage Launch Vehicles," TN D-3191, 1966, NASA.

[4] Teren, F. and Spurlock, O. F., "Optimal Three Dimensional Launch Vehicle Trajectories with Attitude and Attitude Rate Constraints," TN D-5117, 1969, NASA.

[5] Spurlock, O. F. and Teren, F., "A Trajectory Code for Maximizing the Payload of Multistage Launch Vehicles," TN D-4729, 1968, NASA.

[6] Clarke, V. C., Jr., "Constants and Related Data Used in Trajectory Calculations at the Jet Propulsion Laboratory," JPL-TR-32-273, May 1962, Jet Propulsion Lab., California Inst. of Technology, Pasadena, Calif.

[7] Bliss, G. A., *Lectures on the Calculus of Variations*, University of Chicago Press, Chicago, Ill., 1946.

[8] Pontryagin, L. S. et al., *The Mathematical Theory of Optimal Processes*, Interscience, New York, 1962.

[9] Dobson, W. F., Huff, V. N., and Zimmerman, A. V., "Elements and Parameters of the Osculating Orbit and Their Derivatives," TN D-1106, 1962, NASA.

DECEMBER 1971 J. SPACECRAFT VOL. 8, NO. 12

The Critical Dynamic Errors of a Strapdown Guidance System

D. SARGENT* AND H. ZARETT†
TRW Systems, Redondo Beach, Calif.

Strapdown inertial guidance systems have their sensors fixed to the body of the guided vehicle. The system is subjected to vehicle dynamic environments (limit cycle and vibration). Simulations and analyses of one such strapdown system, the Apollo LM Abort Guidance System, were performed to model dynamic errors. There resulted three critical dynamic errors: gyro asymmetry, wheel speed modulation, and coning. The analytic models for these error sources were then verified by test. Dynamic error magnitude predictions were made and implemented into an overall system error model. These predictions were compared to flight results as encountered on the LM lunar mission.

Nomenclature

$A(\Omega_x)$ = gyro loop asymmetry, a function of Ω_x
AGS = Abort Guidance System
ASA = Abort Sensor Assembly, the AGS subassembly containing the sensors and associated electronics
$B(f)$ = computer attenuation function for coning
CSD = cross spectral density
E = "expected value of"
f, f_s = frequency and computer sampling frequency, Hz
$F_1(s), F_2(s)$ = WSM transfer functions
$G_i(s)$ = frequency response of the ith gyro loop
H = gyro wheel angular momentum (2.5×10^5 dyne-cm-sec for AGS)
i,j,k = cyclic permutations of the subscripts, or superscripts, X, Y, and Z
Im = "imaginary part of"
J = gyro float moment of inertia about the output axes, 354 gm-cm² for AGS
LM = Lunar Module
$N(\Omega_x)$ = gyro loop nonlinearity
PGNCS = Primary Guidance, Navigation, and Control System of the LM
PSD = power spectral density
$p(\Omega_x)$ = probability density function of Ω_x
$P_{LC}(\Omega_x)$ = probability density function of the limit cycle part of Ω_x
$p_v(\Omega_x)$ = probability density function of the random vibrational part of Ω_x
PWM = pulse width modulated
RCS = reaction control system
Re = "real part of"
S = Laplace operator, also $S = j\omega = j2\pi f$
SIMU = strapdown inertial measuring unit
SMRD = spin motor rotation detector
T = period of a square wave
TDM = time domain multiplication
WSM = wheel speed modulation
$Y(\Omega_x)$ = gyro loop output including the nonlinearity
α = coning angle

Presented as Paper 70-1029 at the AIAA Guidance, Control and Flight Mechanics Conference, Santa Barbara, Calif., August 17–19, 1970; submitted September 18, 1970; revision received June 3, 1971.

* Section Head.
† Group Leader.

$\dot{\gamma}_i$ = angular rate due to coning about the ith inertial axis
$\dot{\gamma}_{ic}$ = calculated value of $\dot{\gamma}_i$
ΔSF = fractional change in gyro scale factor due to WSM
$\Delta\Omega_{W/C}{}^i$ = angular rate perturbation of the ith gyro wheel with respect to its case
ϵ = fractional gyro scale factor deviation from nominal, asymmetry example
$\sigma_x{}^2$ = variance of the vibrational component of Ω_x
$\dot{\phi}_i$ = angular rate about the ith inertially fixed axis
$\Phi_{\xi\zeta}$ = CSD relating Ω_ξ and Ω_ζ, when ξ and ζ are identical $\Phi_{\xi\xi}$ reduces to a PSD
ω = frequency, rad/sec
ω_0 = coning frequency, rad/sec
Ω = angular rate
Ω_i = angular rate about the ith axis, which is nonstationary in inertial space
Ω_{ioa} = angular rate about the output axis of the ith gyro with respect to inertial space
Ω_I, Ω_0 = angular rate of a gyro case about its input and output axes, respectively, with respect to inertial space
Ω_N = nominal gyro wheel-to-case speed
Ω_{Si} = angular rate of the ith gyro about its spin axis with respect to inertial space
Ω_T = total angular rate at input to $G(S)$
Ω_{test} = angular rate of the test table in WSM test
Ω_x = angular rate at the input to the nonlinearity
$\otimes$ = denotes convolution

Introduction

TO predict the flight performance of a SIMU a mathematical error model which describes system performance must be developed and verified by test. This system error model will consist of a number of component error models each describing a specific error phenomenon. Test data are obtained for each component error resulting in an ensemble statistical estimate for each term. These estimates are combined for each flight phase and the resultant system level mission performance predictions are referred to as the System Capability Estimate.

This paper describes the modeling and verification by test of three critical dynamic errors present in a SIMU of the LM/AGS type: asymmetry, wheel speed modulation, and coning.

Asymmetry

The most important dynamic error source affecting the LM/AGS was found to be gyro asymmetry, which is the even part of the gyro loop input-output curve.

In a strapdown system such as LM/AGS, the output signal from each gyro is used to drive the gyro pickoff signal back to null with constant power pulses. This torquing current is then a measure of the angular rate about the input axis of that gyro. This relationship is usually assumed to be linear. Hence, measurements of the current to each gyro torquer are used by the strapdown system to compute the rotation of a body-fixed coordinate system with respect to an inertially fixed coordinate system. Clearly, if these computations are to be accurate, the relationship between torquer current and input rate must remain linear.

To clarify the effect of gyro nonlinearity on a strapdown system consider a simple example. Assume that the angular rate about the input axis of a gyro is a square wave of magnitude Ω and period T. Further, assume that this gyro can be represented as shown in Fig. 1.

The output of the gyro will also be a square wave, but not an unbiased one as is the input since the net angular displacement measured by the gyro is $T\Omega\epsilon$. As this process repeats every T seconds, this is equivalent to a dynamic gyro drift rate of $\Omega\epsilon$. Note that in a practical situation it is not the vehicle maneuvers, which occur infrequently, but rather the

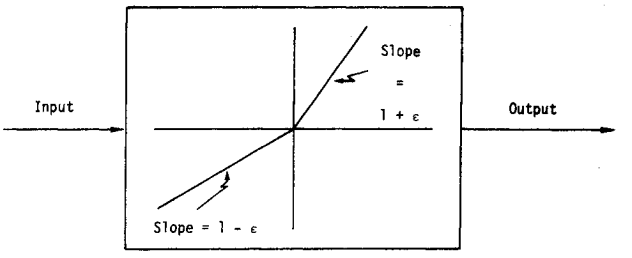

Fig. 1 Example of gyro nonlinearity.

ever present craft limit cycles and random vibrations which cause dynamic drifts when processed by a nonlinear gyro loop.

Consider next the question of how much dynamic gyro drift will be produced by a loop that is not perfectly linear. One model for a gyro loop in which the nonlinearity will cause a dynamic drift but will not have an appreciable effect on loop frequency response is shown in Fig. 2. This model was chosen for its generality. It should be equally applicable to PWM loops such as used in the LM/AGS as well as loops of different design.

Referring to Fig. 2, the total signal, Ω_T sensed by the gyro is the vector sum of two input sources: the angular rate about the gyro input axis and an equivalent input caused by angular accelerations of the gyro case about the gyro output axis. The signal, denoted Ω_x, which is processed by the nonlinearity is this total input signal, modified by the linear gyro frequency response, $G(S)$. For the LM/AGS gyro loop, $G(S)$ is linear and second order with a natural frequency of 24 Hz and damping ratio of 0.43.

During the LM lunar mission, the angular rates Ω_I and Ω_0 were comprised primarily of vehicle limit cycles and random vibration induced by main engine and attitude control jet firings.

To evaluate the dynamic drift caused by the nonlinearity, the probability distribution for the amplitude of Ω_x must be obtained. Then the dynamic drift we seek may be evaluated by

$$\text{Drift} = E[Y(\Omega_x)] = \int_{-\infty}^{\infty} p(\Omega_x) Y(\Omega_x) d\Omega_x \qquad (1)$$

Note that for constant input rates, $JS/H = 0$, $G(S) = 1$, and $\Omega_x = \Omega_I$. Therefore, $Y(\Omega_x)$ can be determined directly by measuring loop output for a selection of constant angular loop input rates.

To obtain $p(\Omega_x)$ for any general input, one must propagate Ω_0 through JS/H, add it vectorially to Ω_I and propagate the vum through $G(S)$ to form Ω_x. This process is explained in setail below for the case where Ω_I and Ω_0 are LM/AGS angular dibrations and limit cycles.

If $p(\Omega_x)$ is an even function of Ω_x (as will prove to be true for the inputs of interest), Eq. (1) may be modified as follows:

$$\text{Drift} = \int_0^{\infty} p(-\Omega_x) Y(-\Omega_x) d\Omega_x + \int_0^{\infty} p(\Omega_x) Y(\Omega_x) d\Omega_x \qquad (2)$$

But for $p(\Omega_x)$ = an even function of Ω_x, $p(\Omega_x) = p(-\Omega_x)$. Therefore

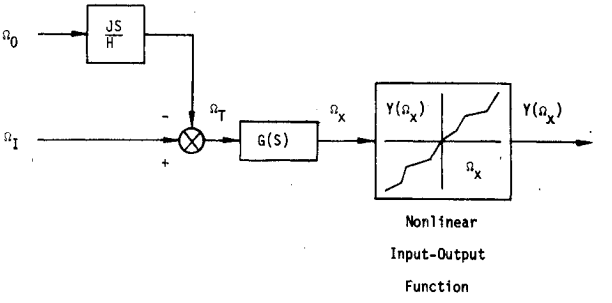

Fig. 2 Model for a gyro with asymmetry.

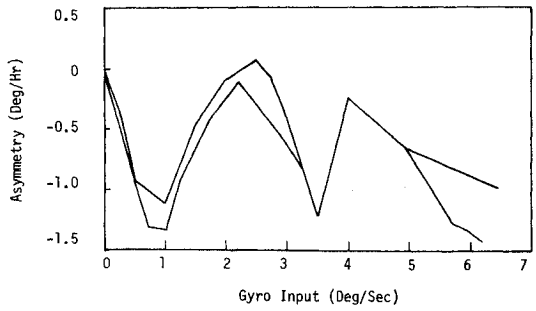

Fig. 3 X-gyro asymmetry, premodification.

$$\text{Drift} = \int_0^\infty [Y(\Omega_x) + Y(-\Omega_x)]p(\Omega_x)d\Omega_x \quad (3)$$

Asymmetry, $A(\Omega_x)$, may now be defined as

$$A(\Omega_x) = [Y(\Omega_x) + Y(-\Omega_x)]/2 \quad (4)$$

and consequently

$$\text{Drift} = 2\int_0^\infty A(\Omega_x)p(\Omega_x)d\Omega_x \quad (5)$$

Asymmetry may also be formulated in terms of nonlinearity, $N(\Omega_x)$, where

$$N(\Omega_x) = Y(\Omega_x) - \Omega_x \quad (6)$$

$$A(\Omega_x) = [N(\Omega_x) + N(-\Omega_x)]/2 \quad (7)$$

Note that Eqs. (4) or (7) define $A(\Omega_x)$ as the even part of either the input-output function, $Y(\Omega_x)$, or of nonlinearity, $N(\Omega_x)$. Clearly, both definitions are equivalent.

Before the asymmetry model described above could be used to predict LM lunar mission performance, it had to be experimentally verified with LM/AGS hardware. To this end a two-part series of tests were conducted on a LM/ASA.

The first part of the test series consisted of constant rate tests to determine the $Y(\Omega_x)$ curves for each ASA gyro. In all cases, the ASA was mounted on a rate table which was driven at a precise angular rate. As the table turned past the zero marker on the table base, a set of electronic gates opened, allowing gyro output pulses to be accumulated by the test equipment. After one or two full revolutions of the table, the same gates closed. The pulse sums were a measure of gyro output, $Y(\Omega_x)$.

Various test orientations of the ASA gyros with respect to the table rotation axis were used. This was done to test the premise that the output of the nonlinearity of any one gyro was determined only by the input to that gyro.

Data from a typical constant rate test is shown in Fig. 3 for the ASA X gyro in terms of asymmetry, and is calculated from Eq. (4) using nominal scale factors to convert pulse counts. Bias and mass unbalance effects were removed from the results.

The lines connecting data points show the upper and lower bounds of the data. Two conclusions were made from these curves. First, no specific orientation or time dependencies were seen. Second, constant rate data was only repeatable to about ±0.2 deg/hr.

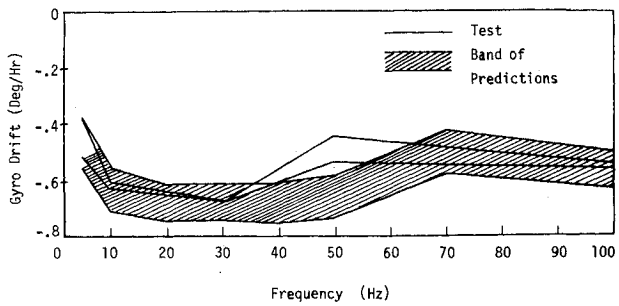

Fig. 4 X-gyro drift, input rate 3.0 deg/sec peak.

The second test series consisted of angular vibration tests performed with the ASA mounted in various orientations on an angular shaker. Sinusoidal vibration runs were made to verify the specific asymmetry frequency dependence depicted in Fig. 2. With the frequency dependence verified, random vibration runs were made to prove the applicabiltiy of the asymmetry model for gyro inputs similar to those expected during the lunar mission. Estimates of expected drift were made for each test run using the asymmetry model of Fig. 2 and both the upper and lower bounds of the asymmetry data as typified by Fig. 3. This led to a band of predictions for each vibration test and is indicative of the limitations on the use of the model due to errors made in data acquisition and to instability of the asymmetry itself.

If an angular rate is applied about only the input or output axis of a gyro, only asymmetry effects about that axis of the gyro are excited. Figure 4 reports prediction and test results from typical sinusoidal tests where input axis effects alone were excited. The two lines for test data represent results obtained from two different test runs. These were made to check repeatability and to validate test data. In general, test results differed from the band of predictions by no more than 0.2 deg/hr. The interested reader will find a full discussion of all test results in Ref. 1.

The predictions and results for cardinal axis random vibration testing are tabulated in Table 1. Two different vibrations levels were applied consecutively about each gyro input axis. Three drift measurements were made at each vibration level for each orientation. The vibration spectra were flat between 40 and 70 Hz with steeply sloping skirts and had Gaussian amplitude distributions. The levels used were 1.81 and 1.35 deg/sec rms.

The asymmetry tests yielded three conclusions: 1) the asymmetry model shown in Fig. 2 can be used to find reasonable estimates of asymmetry drift, however, 2) allowance must be made in any drift prediction for modeling inaccuracies due to instability of constant rate data, imperfect frequency data, and unmodeled effects; and 3) the asymmetry drift during a mission could be intolerably large.

As a result of the above conclusions several modifications were made to the ASA, the AGS computer, and the AGS test equipment. These changes consisted of clock and countdown circuit redesign, and wiring harness and grounding changes.

Table 1 Comparison of prediction test results for random vibration inputs

Gyro	Vibration level, deg/sec rms	Prediction band, deg/hr Lower limit	Prediction band, deg/hr Upper limit	Test results, deg/hr
X	1.81	−0.754	−0.645	−0.860
				−0.881
				−0.892
	1.35	−0.760	−0.675	−0.902
				−0.892
				−0.871
Y	1.81	−0.357	−0.183	−0.304
				−0.283
				−0.336
	1.35	−0.256	−0.105	−0.220
				−0.199
				−0.199
Z	1.81	−0.280	−0.105	−0.283
				−0.273
				−0.325
	1.35	−0.236	−0.073	−0.241
				−0.241
				−0.241

All these modifications served to reduce the amount of intercircuit coupling.

Asymmetry test data from a modified ASA is shown in Fig. 5. Comparison with Fig. 3 shows a dramatic improvement. Asymmetry has been reduced to a tolerable level (0.07 deg/hr, rms). To insure that this level is maintained by all production ASA's, asymmetry data is taken on all units during acceptance testing and used to predict mission performance for each ASA as described below.

In order to predict gyro asymmetry drift during a lunar mission the full angular input to each of the ASA gyros during a mission must be determined. This includes both limit cycle motion and random angular vibration.

A simulation was made of the LM attitude control characteristics with both the PGNCS and the AGS in control of the LM. A worst case (maximum limit-cycle amplitude) curve of amplitude vs time was generated for both LM powered descent and powered ascent. All limit cycles were found to have frequencies less than 10 Hz. The worst case curves for powered descent are shown in Fig. 6. Next, an average probability density curve for the limit cycles about each LM axis during both powered descent and powered ascent was generated. Where it appeared reasonable to do so, the derived probability curves were approximated as Gaussian by equating rms values. Figure 7 shows a comparison of a typical derived curve and its Gaussian approximation.

The LM random vibration spectra were verified by tests at the White Sands Test Facility in New Mexico.[2] The LM was placed in a large vacuum chamber, the navigation base instrumented with angular and linear accelerometers, and the chamber evacuated. Various combinations of reaction control jets were than fired as vibration data was recorded. Next, the descent engine was fired at several different thrust levels and more data were recorded and reduced to yield angular and translational power spectra and cross spectra. Amplitude distributions were also determined and proved to be Gaussian.

The analyses, limit cycles, and vibration spectra described above were combined to yield asymmetry drift estimates for each particular ASA during flight using Eqs. (5) and (7).

The procedure for determining $p(\Omega_x)$, needed in Eq. (5), is as follows (refer to Fig. 2): 1) Find the limit cycle component of Ω_x. Because all limit cycles were low frequency (less than 10 Hz), output axis limit cycles were attenuated by JS/H into insignificance. Input axis limit cycles pass through $G(S)$ unattenuated. Therefore, the limit cycle component of Ω_x is equal to the limit cycle component of Ω_I. 2) Propagate the vibrational part of Ω_0 through JS/H and combine the result with the vibrational part of Ω_I. This yields the vibrational part of Ω_T with Gaussian amplitude distribution and PSD given by Eq. (8).[1]

$$\Phi_{TT}(\omega) = \Phi_{II}(\omega) + [J\omega/H]^2\Phi_{00}(\omega) + 2J\omega\mathrm{Im}[\Phi_{10}(\omega)]/H \quad (8)$$

The PSD of the vibrational part of Ω_x may now be found from

$$\Phi_{XX}(\omega) = \Phi_{TT}|G(S)|^2 \quad (9)$$

This results in a vibrational component of Ω_x that has a Gaussian amplitude distribution with a variance given by

$$\sigma_X^2 = \int_0^\infty \Phi_{XX}(\omega)d\omega \quad (10)$$

where single sided PSD's have been assumed. This fully defines $p_v(\Omega_x)$, the probability density function for the vibration part of Ω_x, to be

$$p_v(\Omega_x) = [\exp(-\Omega_x^2/2\sigma_x^2)]/\sigma_x(2\pi)^{.5} \quad (11)$$

Finally, $p(\Omega_x)$, the probability density function for Ω_x, including vibations and limit cycles is obtained from

$$p(\Omega_x) = p_v(\Omega_x) \otimes p_{LC}(\Omega_x) \quad (12)$$

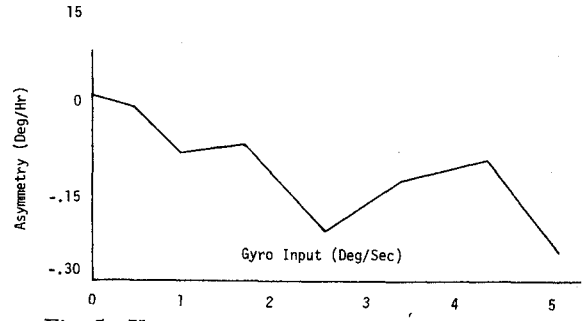

Fig. 5 X-gyro asymmetry, postmodification.

For those cases where $p_{LC}(\Omega_x)$, as well as $p_v(\Omega_x)$, had a Gaussian distribution $p(\Omega_x)$ is also Gaussian with a variance equal to the sum of the variances of the vibrational and limit cycle distributions.

The equations presented above have been incorporated in a computer program that accepts asymmetry data, frequency response data, vibrational PSD's, and limit cycle amplitudes and computes asymmetry drift estimates.

Each set of data will yield one drift estimate for a gyro. An array of 100 drift estimates is calculated, one for each combination of ten limit cycle amplitudes and ten rms values of vibrational power. For both limit cycles and vibration, the ten values used are 10, 20, 30, . . . , 90, and 100% of the maximum, "worst case" values. The mean and rms about the mean of the 100 drift estimates are then calculated. The estimate of asymmetry drift is included in the error model for a particular gyro channel as a Gaussian process with this mean and rms value.

The random component about the mean allows for the fact that before any given LM flight there is no way to tell if thrust vector misalignments and RCS jet unbalances will conspire to yield a smooth LM flight or one with near maximum limit cycling and vibration.

Wheel Speed Modulation

The second dynamic error of interest is wheel speed modulation (WSM) which may cause the gyros in a strapdown inertial system to drift significantly in the presence of sustained low-frequency oscillations. To understand this phenomenon consider the behavior of a gyro subjected to oscillations of its case about its spin axis. The spin motor tends to maintain the gyro wheel rotating at a constant rate with respect to its case. For very low-frequency case oscillations (1 Hz or less) the gyro will operate as intended and the wheel will follow the case oscillations. That is, it will speed up and slow down with respect to inertial space. If very high-frequency case motion were applied however, the inertia of the wheel would preclude its following the case oscillations. The wheel would continue to rotate at a constant rate with respect to inertial space.

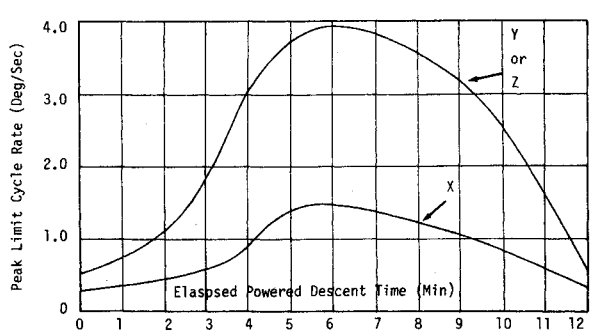

Fig. 6 Maximum zero to peak limit cycle rates during powered descent, sinusoidal waveform.

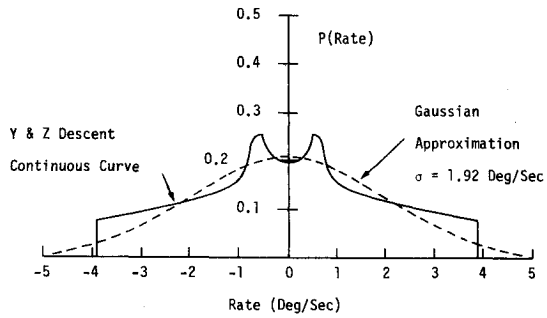

Fig. 7 *Y* and *Z* descent probability distribution.

At some frequency in between these two extremes there exists a resonance. For the LM ASA gyros, this resonance occurs at about 3 Hz. Because of the very light damping that exists between a gyro wheel and its float, the resonance is extremely sharp and the magnitude of the wheel oscillations is many times that of the case oscillations.

When three gyros are configured in a strapdown system, this resonance phenomenon occurs with an added complication. It is common for all three gyros to share one spin motor power supply. The ac output impedance of such a supply will not be zero. When one gyro wheel is perturbed due to spin axis case motions, current surges will be drawn from the supply and the other gyro wheels. Consequently, if one gyro is perturbed, all will be perturbed and multiple resonance points occur.

Perturbations of the gyro wheel spin rate represent changes in gyro wheel angular momentum, and hence the scale factor of the gyro loop. If an oscillation of the same frequency as the wheel speed perturbations is simultaneously applied to the gyro input axis, a rectification error (dynamic drift) will occur.

If the wheel speed perturbations are denoted by $\Delta\Omega_{W/C}$ and the nominal wheel-to-case speed is denoted by Ω_N, then the fractional change in scale factor, ΔSF caused by WSM is given by

$$\Delta SF = \Delta\Omega_{W/C}/\Omega_N \tag{13}$$

and as $\Delta\Omega_{W/C}$ oscillates, so does ΔSF. If the input to the gyro Ω_I also oscillates at the same frequency a drift will result. Assume $\Omega_I = A \sin\omega_0 t$ and $\Delta\Omega_{W/C} = B \sin(\omega_0 t + \phi)$. This situation is depicted in Fig. 8.

$$\begin{aligned}\text{Loop Output} &= A \sin\omega_0 t[SF + \Delta SF] \\ &= A \sin\omega_0 t[SF + (B/\Omega_N) \sin(\omega_0 t + \phi)]\end{aligned} \tag{14}$$

and this quantity has a nonzero average value (dynamic drift) equal to

$$\text{Drift} = \langle \Omega_I(t) \Delta SF(t) \rangle = AB \ (\cos\phi)/2\Omega_N \tag{15}$$

The model developed to relate wheel speed perturbations of one gyro to case motions of all three gyros is:

$$\Delta\Omega_{W/C^i} = F_1(S)\Omega_S{}^i + F_2(S)[\Omega_S{}^j + \Omega_S{}^k] \tag{16}$$

To determine the characteristics of F_1 and F_2, including the question of their linearity (or lack of it), an ASA was mounted on a rate table in various orientations with respect to the axis of rotation of the table. The table was driven in a closed loop

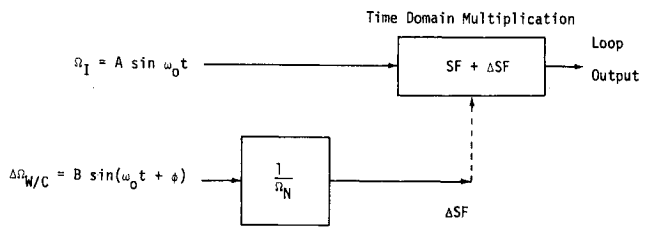

Fig. 8 The WSM drift mechanism.

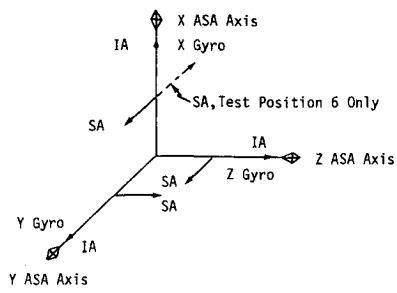

Fig. 9 Orientation of ASA gyro axes.

manner by a high precision, low frequency, sinusoidal oscillator. Amplitudes of wheel speed perturbations and dynamic gyro drifts were measured at various amplitudes in the 0 to 10 Hz range. The wheel speed perturbation amplitudes were measured by monitoring the SMRD. The dynamic drifts were reduced by collecting gyro pulses for a set time period with the table oscillating and again with it still. The difference in pulse counts was proportional to dynamic drift. The details of these data acquisition techniques can be found in Ref. 4. Figure 9 shows the orientation of the spin and input axes of the gyros when mounted in the ASA. The six test positions are described in Table 2.

For each test position, the angular rate of each ASA gyro case about its spin axis Ω_S may be determined by simultaneous examination of Table 2 and Fig. 9. The hypothesized wheel speed perturbations, $\Delta\Omega_{W/C}$ for each test position can then be found from Eq. 16. This information is presented in Table 3.

The test results may be summarized as follows: 1) For the input amplitudes expected during mission (less than 6 deg/sec for almost the whole flight) the WSM phenomenon was found to be linear. 2) In general two resonances were evident, one at 3.0 Hz, and the other at 4.0 Hz. 3) The wheel speed perturbation curves repeated as predicted by Table 3 (e.g., $\Delta\Omega_{W/C}{}^X$, test position 3 looked very much like $2\Delta\Omega_{W/C}{}^Y$, test position 2, as a function of frequency). This provided partial substantiation of the model. 4) In test position 4, the 4.0 Hz resonance was not observed. This meant the transfer $F_1 + 2F_2$ did not contain a 4.0 Hz resonance. Further, at 3.0 Hz a phase shift of $-35°$ in $F_1 + 2F_2$ was indicated in the drift data, exclusive of the sharp 180° phase shift which accompanies a resonant peak. 5) In test position 6, the 3.0 Hz resonance was not observed. Consequently, the transfer function $F_1 - F_2$ did not contain this resonance.

The test findings stated above and the endpoint conditions listed below sufficed to define $F_1(S)$ and $F_2(S)$. The endpoint conditions are as follows: 1) Step changes of gyro case angle or rate about the spin axis will cause only transient perturbations in all gyros. Therefore, $\lim_{s\to 0} F_1(S) = 0$, $\lim_{s\to 0} F_2(S) = 0$. 2) Due to wheel inertia, the wheels will not be perturbed with respect to their constant rotation in inertial space, in the presence of high frequency case oscillations. That is, the case of the oscillating gyro is perturbed in inertial space, the wheel is not. Consequently, $\lim_{s\to\infty} F_1(S) = -1$, $\lim_{s\to\infty} F_2(S) = 0$.

The simplest way to derive transfer functions which meet all of the endpoint conditions and also match the test data is

Table 2 Description of test positions

Test position	Table axis of rotation
1	Along *X* ASA axis
2	Along *Y* ASA axis
3	Along *Z* ASA axis
4	In *YZ* plane, 45° to both $+Y$ and $+Z$ axes
5	In *YZ* plane, 45° to both $+Y$ and $-Z$ axes
6	Along *Y* ASA axis with *X* gryo turned 180° about input axis in mounting hole

Table 3 Normalized gyro spin axis angular rates and resultant wheel speed perturbations: WSM test

Test position	$\frac{\Omega_S{}^X}{\Omega_{test}}$	$\frac{\Omega_S{}^Y}{\Omega_{test}}$	$\frac{\Omega_S{}^Z}{\Omega_{test}}$	$\frac{\Delta\Omega_{W/C}{}^X}{\Omega_{test}}$	$\frac{\Delta\Omega_{W/C}{}^Y}{\Omega_{test}}$	$\frac{\Delta\Omega_{W/C}{}^Z}{\Omega_{test}}$
1	0	0	0	0	0	0
2	1	0	1	$F_1 + F_2$	$2F_2$	$F_1 + F_2$
3	0	1	0	F_2	F_1	F_2
4	0.707	0.707	0.707	$0.707(F_1 + 2F_2)$	$0.707(F_1 + 2F_2)$	$0.707(F_1 + 2F_2)$
5	0.707	0.707	0.707	$0.707F_1$	$0.707(F_1 - F_2)$	$0.707F_1$
6	−1	0	1	$-(F_1 - F_2)$	0	$F_1 - F_2$

to assume the form for $F_1 + 2F_2$ and $F_1 - F_2$ given by Eqs. (19) and (20), respectively

$$F_1(S) + 2F_2(S) = \frac{-S^2(S + A)}{(S^2 + 2\zeta_1\omega_1 S + \omega_1{}^2)(S + B)} \quad (19)$$

$$F_1(S) - F_2(S) = -S^2/(S^2 + 2\zeta_2\omega_2 S + \omega_2{}^2) \quad (20)$$

The constants A and B were chosen to yield a maximum phase shift due to $(S + A)/(S + B)$ of −35° at 3.0 Hz. There resulted: $A = 35.17, B = 9.80$. The known resonances must correspond to ω_1 and ω_2; therefore, $\omega_1 = 2\pi(3.0) = 18.87$, $\omega_2 = 2\pi(4.0) = 25.15$. Values of ζ_1 and ζ_2 were chosen to match the data at resonance from testing positions 4 and 3, respectively. The values were: $\zeta_1 = 0.1667$ and $\zeta_2 = 0.0063$. These values were substituted into Eqs. (19) and (20) which were then solved for F_1 and F_2.

A comparison for a typical gyro channel of measured and predicted wheel speed perturbations based on Eq. (19) and (20) is shown in Fig. 10. The predictions and data are normalized to Ω_{test}.

The general WSM error model for the ith ASA gyro applicable to the LM lunar mission is shown in Fig. 11. To predict mission drift, the limit cycle inputs and the angular vibration profiles were applied to the WSM error model. The limit cycles were deterministic and drift estimates were made by straightforward application of Fig. 11.

The vibration spectra all had neligible power in the frequency range below 20 Hz. Conversely, above 20 Hz, $F_1(S) \cong -1$ and $F_2(S) \cong 0$. Therefore, the WSM error model for vibration reduced to that shown in Fig. 12.

It can be shown[4] that the drift may be evaluated by Eq. (21)

$$\text{Drift} = \frac{-1}{\Omega_N}\int_0^\infty Re[\Phi_{IS}(\omega)]d\omega \quad (21)$$

Note that single sided PSD's have again been assumed.

Calculations showed that WSM error would be very small except when the LM limit cycled at 3.0 or 4.0 Hz. Simulations showed that the 3.0 to 4.0 Hz range would be excited during the powered ascent portion of the LM mission but only for about 50 sec. A worst case error was calculated (i.e., a dwell at 3.0 Hz for 50 sec) and averaged over the full time of powered ascent and found to be 0.075 deg/hr, a tolerable number.

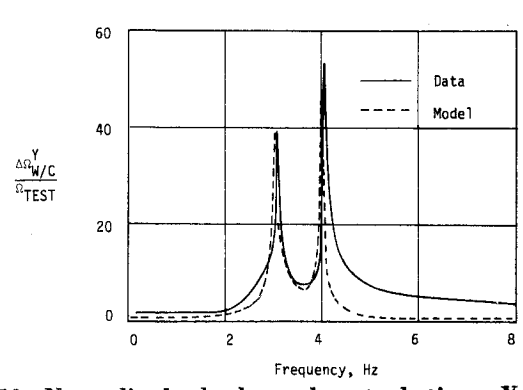

Fig. 10 Normalized wheel speed perturbations, Y gyro, position 2.

Coning

Coning is a well-known phenomenon, discussed in literature dating back to 1958. The equations for coning can be derived directly from the principles of dynamics.[5,6] It can be shown[7] that for small angular motions Eqs. (22) and (23) describe the relationship between angular rates about a set of three orthogonal inertially fixed axes and a second set of three orthogonal angularly rotating axes.

$$\dot{\gamma}_i = \tfrac{1}{2}(\phi_j\dot{\phi}_k - \phi_k\dot{\phi}_j) \quad (22)$$

$$\dot{\phi}_i = \Omega_i + \dot{\gamma}_i \quad (23)$$

It may be shown[7] that where small angle approximations are valid, Eq. (22) may be restated in terms of body rates (i.e., the Ω_i) as

$$\dot{\gamma}_i \simeq \tfrac{1}{2}(\theta_j\Omega_k - \theta_k\Omega_j),\ \theta_i = \int_0^t \Omega_i dt \quad (24)$$

and θ_i is restricted to be a small angle.

To better visualize the process just described, consider Fig. 13. Assume that a SIMU is fixed in the X, Y, Z frame. The X axis traces out a cone in inertial space. After one full cycle, the X, Y, Z axes have returned to their initial orientations.

It is shown[8] that if at $t = 0$ the X axis lies in the X_{nom}, Y_{nom} plane, then the three strapdown gyros with input axes along the X, Y, and Z axes would measure, respectively

$$\Omega_X = -\Omega^2/2\omega_0,\ \Omega_Y = -\Omega\cos(\omega_0 t),\ \Omega_Z = -\Omega\sin(\omega_0 t) \quad (25)$$

where ω_0 is the coning frequency. The angle α shown in Fig. 13 is called the coning angle and had a magnitude of Ω/ω_0.

Note that if Eq. (25) is substituted into Eqs. (24) and (22) to evaluate $\dot{\phi}_x$ the result is zero, as expected. Consideration of each body rate of Eq. (25) separately would not have led to this conclusion.

Strapdown inertial systems must have a computer, programmed with an algorithm which processes measured body rates simultaneously. The LM/AGS uses a direction cosine update algorithm which performs this function. There are several reasons, however, why such an algorithm will not perform perfect calculations and these imperfections lead to coning errors.

There are three major causes of coning error, all of which stem from the processing of sinusoidal rates, [e.g., Ω_Y and Ω_Z in Eq. (25)]. These causes are: 1) Nonunity gyro loop frequency response. Typical loops will yield faithful measure-

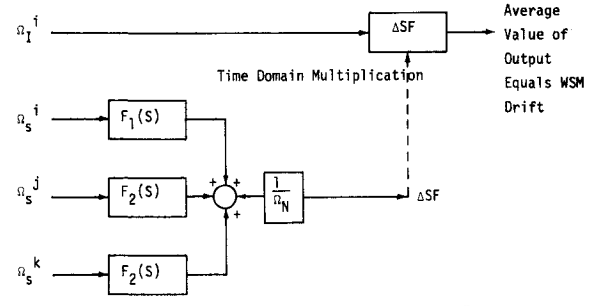

Fig. 11 Full WSM error model.

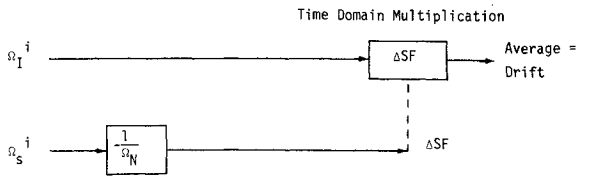

Fig. 12 High frequency WSM error model.

ments of low-frequency inputs, amplified measurements of mid-frequency inputs, and attenuated measurements of high-frequency inputs. 2) Computer attenuation due to non-infinite sampling rate. Studies have shown[9] that use of a sampling frequency of f_s Hz results in a computed coning rate equal to

$$\dot{\gamma}_{ic} = \dot{\gamma}_i[\sin(2\pi f/f_s)/(2\pi f/f_s)] \equiv \dot{\gamma}_i B(f) \qquad (26)$$

where $\dot{\gamma}_i$ is given by Eq. (24) and f is the coning frequency [i.e., $\omega_0/2\pi$ in Eq. (25)]. 3) Gyro output axis coupling. As shown in Fig. 2 the output of a gyro loop will indicate both the angular rate about its input axis and the negative of the angular acceleration about its output axis (scaled by J/H).

The coning error mechanism for one strapdown gyro channel incorporating all these factors is depicted in Fig. 14. The error is defined as the calculated coning rate $\dot{\gamma}_{ic}$ less the actual coning rate $\dot{\gamma}_i$ given by Eq. (24).

Although the coning error model depicted in Fig. 14 is formidable in appearance, its use with deterministic inputs is straightforward. If, however, the angular rates $\Omega_{i,j,k}$ are correlated random vibrations then the calculations of the coning rate error may be shown to reduce to the evaluation of Eq. (27) below[4]

$\dot{i}$-channel coning rate error =

$$\int_0^\infty Re\left[\Phi_{j,k}\frac{1}{S}[1 - G_j(-S)G_k(S)B(f)]\right]d\omega +$$
$$\int_0^\infty Re\left[\Phi_{j,koa}\frac{J}{H}G_j(-S)G_k(S)B(f)\right]d\omega -$$
$$\int_0^\infty Re\left[\Phi_{k,joa}\frac{J}{H}G_j(S)G_k(-S)B(f)\right]d\omega +$$
$$\int_0^\infty Re\left[\Phi_{joa,koa}\left(\frac{J^2}{H}\right)SG_j(-S)G_k(S)B(f)\right]d\omega \qquad (27)$$

Again, single sided spectra have been assumed.

The first integral in Eq. (27) is the coning error caused by imperfect calculation of actual coning motion. The other three integrals represent various forms of output axis acceleration coupling which is erroneously interpreted by the system to be coning motion. These three integrals are sometimes referred to as pseudo-coning errors.

Before LM/AGS, coning theory had never been fully verified by test. A special coning table was designed to impart angular motion to a body mounted on it similar to that depicted in Fig. 13. [The one difference was that one of the horizontal nonstationary axes was constrained to move in a vertical plane. Referring to Fig. 13, this would cause the X gyro to sense an angular rate which varies as $\sin(2\omega_0 t)$ as well as the constant rate given in Eq. (25).]

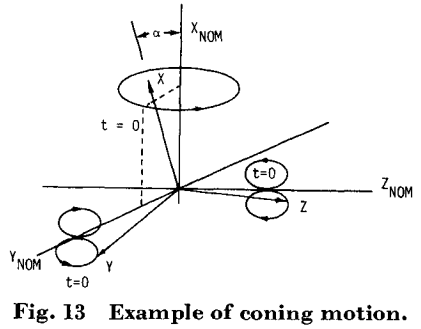

Fig. 13 Example of coning motion.

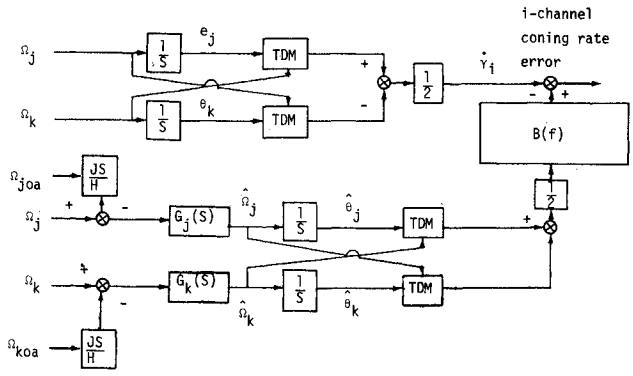

Fig. 14 The coning error mechanism.

The test consisted of mounting an ASA on the coning table in various orientations, and with the computer operating, applying sinusoidal coning motion at various amplitudes and frequencies to the ASA. Predictions of coning rate error were made for each gyro for each test run using the coning error model depicted in Fig. 14. The drift rates as determined by the computer were then compared with predictions.

The conclusions of this testing were: 1) The coning error mechanism of Fig. 14 faithfully predicts coning error, and 2) the computer attenuation function, $B(f)$ is well modeled by Eq. (26).

The results of the LM limit cycle simulation studies showed that limit cycling would induce an insignificant coning error during the lunar mission. This was due primarily to the fact that most limit cycling would be in the 0–5 Hz range and all would be in the 0–10 Hz range.

The LM specification vibration spectra (based on the results of the White Sands test) were used to evaluate Eq. (27) for all three gyro channels. These calculations showed that: 1) Coning due to output axis to output axis coupling [the last integral in Eq. (27)] was negligible. 2) Coning error during mission was expected to be small—less than 0.07 deg/hr rms.

Dynamic Performance

The LM powered flight dynamic environments were separated into descent and ascent phases. The AGS dynamic drift values were estimated for each flight phase. Table 4 shows a comparison of preflight predicted dynamic drifts and measured inflight drift values as encountered on the manned Apollo Flights 10, 11, and 12. The predicted drift values are based on ensemble performance capability estimates[10] and on individual flight systems asymmetry scale factor measurements. The ensemble 3σ values are based on test data from

Table 4 Apollo flight gyro dynamic drift, deg/hr

Flight		Predicted mean	Predicted 3σ	Measured inflight mean
Apollo 10	X	−0.12	0.49	−0.13
(Powered ascent)	Y	−0.14	0.35	−0.06
	Z	0.08	0.35	0.17
Apollo 11	X	0.02	0.32	−0.02
(Powered descent)	Y	−0.10	0.27	−0.03
	Z	0.02	0.26	0.38
Apollo 12	X	−0.08	0.37	0.05
(Powered descent)	Y	−0.16	0.27	−0.17
	Z	0.07	0.26	0.08
Apollo 12	X	−0.09	0.45	0.30
(Powered ascent)	Y	−0.14	0.32	−0.40
	Z	−0.28	0.41	−0.46

sixteen systems tested over a period of three years. These values include all dynamic errors. The predicted mean values are derived directly from the asymmetry program described earlier.

The measured inflight dynamic drift values were obtained from postflight data analysis. These analyses consisted of performing a least squares curve fit to the integrated PGNCS/AGS body rate differences over the applicable flight phases. It was assumed that no errors existed in the PGNCS data. This technique results in a postflight best estimate of AGS performance relative to PGNCS. The uncertainties associated with each estimate include PGNCS drift errors, data readout quantization errors, and sampling and processing errors. These errors are discussed in Ref. 11.

Considering the uncertainties due to measurement and processing errors associated with the inflight error estimates, the inflight mean values are compatible with the distribution of the ensemble capability estimates.

Summary and Conclusions

This paper has reported on the work accomplished evaluating the critical dynamic errors of the LM/AGS Strapdown Guidance System. The error models can generally be applied to any strapdown guidance system having sensors of the type used on the AGS.

The important findings were: 1) Inflight error measurements agree with preflight estimates, indicating no significant unmodeled error sources exist in the LM/AGS. 2) Asymmetry, wheel speed modulation, and coning errors are dependent on power spectra and cross spectra of vehicle motion and vibration. This dependency can be adequately modeled. 3) Models for these dynamic error sources have been verified by laboratory test. 4) Asymmetry errors induced by extraneous ground loops and mixing of power and signal grounding paths can be minimized through careful desing. 5) Although strapdown system capability has been proved, the intentional uncoupling of strapdown components should circumvent many interesting technical surprises in future (more sophisticated) strapdown systems.

References

[1] Sargent, D., Wolterbeek, H., Weber, T., Massey, E., "LM Abort Sensor Assembly Gyro Rate Measurement Asymmetry; Model & Tests," 03358-6053-R000, Nov. 22, 1967, TRW Systems, Redondo Beach, Calif.

[2] Irwin, H., "White Sands Test Facility Abort Sensor Assembly Vibration Test Report," 03358-6046-R000, July 5, 1967, TRW Systems, Redondo Beach, Calif.

[3] Bregman, D. and Wolterbeek, H., "H-Vector Spin Input Rectification," 03358-6139-T000, Dec. 2, 1968, TRW Systems, Redondo Beach, Calif.

[4] Sargent, D. and Rountree, R., "Rectification Errors in Strapdown Inertial Components due to Random Vibrations," *Proceedings of Third Inertial Guidance Test Symposium*, Vol. I, 1966, Air Force Missile Development Center, Holloman Air Force Base, N. Mex.

[5] Goodman, L. and Robinson, A., "Effects of Finite Rotations of Gyroscopic Sensing Devices," *Journal of Applied Mechanics*, Vol. 25, No. 2, June 1968, pp. 210–213.

[6] Cannon, R., "Kinematic Drift of Single Axis Gyroscopes," *Journal of Applied Mechanics*, Vol. 25, No. 3, Sept. 1968, pp. 357–360.

[7] Wirth, E., "Equations for Strapped Down Attitude Reference Errors," IOC 7222.6-77, Nov. 21, 1966, TRW Systems, Redondo Beach, Calif.

[8] Bregman, D., "Analysis of a Coning Table," IOC 7222.8-67, July 28, 1966, TRW Systems, Redondo Beach, Calif.

[9] Baker, K., "Analytic Platform Coning Study Results," IOC 7222.7-68, July 13, 1966, TRW Systems, Redondo Beach, Calif.

[10] Zarett, H., "LM AGS Capability Estimate," 03358-6134-R000, Revised Dec. 31, 1969, TRW Systems, Redondo Beach, Calif.

[11] Mason, W. and Wedekind, D., "Prediction & Measurement of Strapdown Inertial Measurement Unit Performance on Lunar Mssions," *Proceedings of the AIAA Guidance & Control Conference*, AIAA Paper 70-1028, 1970.